Analytica Chimica Acta 1086 (2019) 133–141

Contents lists available at ScienceDirect

Analytica Chimica Acta

journal homepage: www.elsevier.com/locate/aca

Thermodynamics-based retention maps to guide column choices for comprehensive multi-dimensional gas chromatography

Keisean A.J.M. Stevenson [a], Leonid M. Blumberg [b], James J. Harynuk [a, *]

[a] Department of Chemistry, University of Alberta, Edmonton, AB, T6G 2G2, Canada
[b] Advachrom, P.O. Box 1243, Wilmington, DE, 19801, USA

HIGHLIGHTS

- Novel application of distribution-centric 3-parameter thermodynamic model of GC.
- Rapidly evaluate column combinations for GC × GC before buying columns.
- Extends easily to GC × GC × GC separations.

GRAPHICAL ABSTRACT

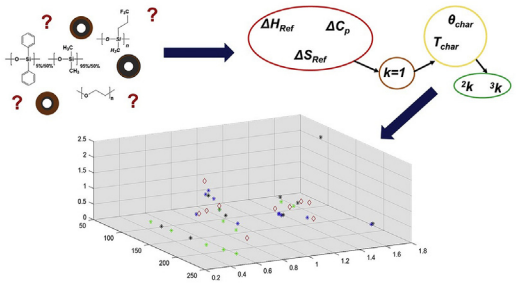

ARTICLE INFO

Article history:
Received 6 May 2019
Received in revised form
1 August 2019
Accepted 2 August 2019
Available online 7 August 2019

Keywords:
Column selection
Comprehensive multi-dimensional gas chromatography
Retention maps
Thermodynamic models
GC×GC

ABSTRACT

Comprehensive two-dimensional gas chromatography (GC × GC) provides enhanced separation power over its one-dimensional counterpart – gas chromatography (GC). This enhancement is achieved by the inclusion of a secondary column, the choice of which is a major determinant on the quality of the ultimate separation. When developing and optimizing a new GC × GC method, the choices of stationary phase chemistries, geometries and configurations (which phase serves in which dimension) are of fundamental importance, and must often be addressed even before the manipulation of instrumental conditions. These choices are often made using educated guesses, literature searches, or trial and error. Thermodynamic models of GC separations; however, provide a fast and easy means of acquiring information for guiding these choices. By using characteristic thermodynamic parameters (characteristic temperatures, T_{char}, and characteristic thermal constants, θ_{char}), we demonstrate the generation of maps that can inform the choices of column chemistries, phase ratios and configurations for GC × GC separations.

1. Introduction

Comprehensive two-dimensional gas chromatography (GC × GC) allows chemists to separate and analyse complex samples that are difficult or often impossible to resolve by traditional gas chromatography (GC). The addition of a secondary column that separates analytes via a different mechanism than the primary column, and which is coupled to the primary column by means of a modulator delivers the extra separation. Overall, a greater peak capacity results. Despite the added separating power, developing and optimizing a GC × GC method is a complicated task as the various parameters that may be manipulated influence multiple other parameters, which are coupled through a series of complex

* Corresponding author.
E-mail address: james.harynuk@ualberta.ca (J.J. Harynuk).

https://doi.org/10.1016/j.aca.2019.08.011
0003-2670/

relationships [1]. However, prior to optimizing pneumatic and temperature conditions, the chromatographer has to answer the questions of which two stationary phase chemistries would be ideal for meeting the goals of the separation, in what order should said phases be configured, and which phase ratios should be used in each dimension to achieve the desired resolution. Optimization of these parameters is expensive in terms of time and resources, as multiple columns may need to be purchased, and changing geometric parameters of the columns requires instrument shutdowns to physically change its configuration.

Thermodynamics-based predictive models have been successfully used throughout the literature to simulate and predict GC [2–12] and GC × GC separations [13–18]. As such, they provide a useful place to start for development of a fast, simple, reliable and convenient way to answer questions pertaining to column chemistry and geometry choice. Typically, researchers in the area of thermodynamics-based modelling of GC rely on the three-parameter model, based on the work of Clarke and Glew [19], which relates distribution coefficients, K, to absolute temperature, T.

$$\ln K = A + \frac{B}{T} + C \ln T \tag{1}$$

Values of A, B and C are acquired through curve-fitting/numerical optimization procedures performed on experimentally obtained retention data of compounds of interest obtained under various conditions. These parameters allow the calculation of values representing the thermodynamic parameters, ΔH_{ref}, ΔS_{ref} and ΔC_p [5,7,14,20–23]. These are the changes in enthalphy, entropy and isobaric molar heat capacity, respectively, associated with the partitioning of an analyte between the mobile and stationary phases, defined at some arbitrary reference temperature, T_{ref}:

$$\Delta S_{ref} = R\left(A + C + C\ln T_{ref}\right) \tag{2}$$

$$\Delta H_{ref} = -R\left(B + CT_{ref}\right) \tag{3}$$

$$\Delta C_p = RC \tag{4}$$

When defined this way, the model may be described as temperature centric (T-centric).

Such an approach to modelling retention in GC systems is useful and justified but falls short in some regards. The values of ΔS_{ref} and ΔH_{ref} depend on the arbitrarily chosen value of T_{ref} and it is often desirable and computationally efficient to select the same T_{ref} for all analytes. However, at a given T_{ref} there will be analytes whose retention factors, k, are chromatographically meaningless. For example, if a moderate oven temperature such as 90 °C is chosen as T_{ref}, a very volatile molecule like butane (boiling point, ~ −1 °C) injected onto a highly polar, wall-coated ionic liquid column would have an extremely small value for k and would pass through the column with little-to-no interaction with the stationary phase. One could not fairly describe its progression through the column as chromatography. On the other hand, a large and heavy PAH such as benzo[a]pyrene (boiling point, 495 °C) injected onto a poly(90% biscyanopropyl/10% cyanopropylphenyl siloxane) column would be expected to have a k so large at 90 °C that it would focus at the head of the column, and remain there indefinitely. Neither of these two scenarios is uncommon with real samples, and so an alternative and more meaningful approach is desirable. By choosing instead the same reference distribution coefficient, K_{Ref}, for all analytes and calculate a different T_{Ref} for each compound such that T_{Ref} is the temperature at which $K = K_{Ref}$. This would generate thermodynamic parameters that are analyte-dependent and as such are more relevant for the analyte(s) under consideration. When modelled this way, the approach is described as being distribution-centric (K-centric) [23] and the uppercase subscript "$_{Ref}$" is used to represent the reference parameters based on the same K_{Ref} for all analytes. The resulting distribution-centric 3-parameter model is given by Equation (5) below where K-centric parameters ΔH_{Ref} and ΔS_{Ref} are calculated from parameters A, B and C [23]

$$\ln K = \frac{\Delta S_{Ref}}{R} - \frac{\Delta H_{Ref}}{RT} + \frac{\Delta C_p}{RT}\left(T - \frac{\Delta H_{Ref}}{\Delta S_{Ref} - R\ln K_{Ref}}\right) + \frac{\Delta C_p}{R}\ln\left(\frac{\left(\Delta S_{Ref} - R\ln K_{Ref}\right)T}{\Delta H_{Ref}}\right) \tag{5}$$

This paper presents the use of thermodynamic parameters that result from this K-centric approach to generate maps of analyte distribution in GC × GC separation spaces formed from different combinations of stationary phase chemistries, phase ratios and configurations.

1.1. Theory

Equation (5) forms the basis of the model, but another important parameter must be introduced; that is the thermal constant of analyte-column interaction, θ. This parameter, analogous to parameters such as time constants and half-lives, represents the temperature change in either direction that would cause an e-fold (e = Euler's number, ~2.72) change in distribution coefficient, K, and in retention factor, k, in the opposite direction. It is defined in Equation (6) below [24,25]:

$$\theta = -\left(\frac{d\ln k}{dT}\right)^{-1} \tag{6}$$

θ is a very convenient and versatile parameter as it always has the same value regardless of how the relationship between k and T is expressed (e.g. k vs T, $ln\ k$ vs T, $log\ k$ vs T, etc.) and when written as shown in Equation (6), has the convenient units of temperature (°C). It will prove crucial to the work demonstrated in this paper. The value of θ at $T = T_{Ref}$ is denoted below as θ_{Ref}.

In order to begin using the distribution-centric model for guiding column choices in GC × GC, the question of where to set K_{Ref}, needs to be answered. For the sake of mathematical simplicity, K_{Ref} can be set to give a temperature, T_{Ref}, for each analyte such that $k = k_{Ref} = 1$.

Recalling that:

$$K = k\beta \tag{7}$$

where β is the column phase ratio. Therefore, when $k = 1$, $K = \beta$. For a given analyte, the reference temperature, $T_{Ref,}$ and reference thermal constant, θ_{Ref}, are termed the characteristic temperatures, $T_{char,}$ and characteristic thermal constant, θ_{char}, respectively [24,25].

If the parameters A, B and C, for an analyte of interest are known, we can obtain T_{char} and θ_{char} by way of the Lambert W function [23].

$$T_{char} = -\frac{B}{CW(x)} \tag{8}$$

$$\theta_{char} = \frac{B}{C^2(1 + W(x))W(x)} \tag{9}$$

where W(x) is the Lambert W-function of x given by:

$$x = -\frac{Be^{\frac{A}{C}}}{CT_1\beta^{\frac{1}{C}}} \quad (10)$$

T_1 is the base unit of temperature (1 K). A solute retention factor, k, can be expressed via its characteristic parameters [23]:

$$\ln k = \left(C + \frac{T_{char}}{\theta_{char}}\right)\frac{T_{char} - T}{T} + C\ln\frac{T}{T_{char}} \quad (11)$$

The two characteristic parameters, T_{char} and θ_{char} help us model analyte distribution in GC × GC separations and rapidly generate maps which can be used to help with column selection. During a relatively long single-ramp temperature-programmed GC separation, all analytes elute from the column with about the same retention factor [24,26]. An analyte's elution temperature from a GC column, T_e, is strongly correlated with its characteristic temperature, T_{char} [23]. (generally, T_e increases with increasing T_{char}). For closely eluting analytes, the difference in their elution temperatures is related to their respective θ_{char} [25]. Deviations from these trends are relatively minor and previous studies have suggested that at any heating rate, analytes elute in order of increasing T_{char} [23–25]. It was therefore hypothesized that characteristic parameters for a given set of analytes can be used to provide a map of how analytes will distribute across a GC × GC separation space and by extension, provide insight into how stationary phase chemistry, phase ratios and configurations will influence said distribution.

The temperature during a single-ramp temperature-programmed GC experiment can be described as:

$$T = T_i + R_T t \quad (12)$$

where T_i is the initial oven temperature (°C), R_T is the column heating rate (°C min^{-1}) and t is time (min). Characteristic thermal constants may be used as basic temperature units [24], void times may be used as basic time units [27], and R_T can be expressed as:

$$R_T = r\frac{\theta_{char}}{t_M} \quad (13)$$

where r is a dimensionless parameter that can be interpreted as the dimensionless heating rate [24,25,28].

The following considerations allow one to estimate numerical values of parameters in Eq (13).

It is convenient to compare numerical values of solute parameters under identical conditions. One of such conditions is a column phase ratio (β). It is assumed below that, unless otherwise is explicitly stated, $\beta = 250$ (i.e. the ratio of film thickness to column internal diameter is 0.001).

Characteristic thermal constants (θ_{char}) of different solutes can range (in a column with $\beta = 250$) somewhere between 20 °C and 40 °C [25]. Different solutes having the same T_{char} can have different θ_{char}. However, as a general trend, solutes having larger T_{char} have larger θ_{char}. As a result, θ_{char} value of eluting solute increases during the heating ramp. The trend of generally larger θ_{char} for the solute having larger T_{char} can be expressed for the columns with $\beta = 250$ regardless of combinations of column and analyte polarities as [25,28]:

$$\theta_{char,nom} = 22°C\left(\frac{T_{char}}{273.15\ K}\right)^{0.7},\ (\beta = 250) \quad (14)$$

where $\theta_{char,nom}$ is the nominal (expected) value of θ_{char} for a solute having a given T_{char}. The actual θ_{char} values overwhenlimng majority of solute-column combinations are confined at each T_{char} within the bounds [25]:

$$0.7\theta_{char,nom} \le \theta_{char} \le 1.3\theta_{char,nom} \quad (15)$$

In addition to temperature-dependent θ_{char}, the void time (t_M) in Eq. (13) also depends on temperature. It is convenient therefore, to choose a single predetermined temperature for the measurement of t_M and selection of θ_{char} in Eq. (13). Such temperature can be 150 °C – a round number in about the middle of the common GC temperature range [28]. One can find from Eq. (14) that, at $T_{char} = 150$ °C, the nominal value of θ_{char} is close to 30 °C [25,28]. Eq. (13) becomes:

$$R_T = r\frac{30°C}{t_M},\ (\text{at}\ \beta = 250, \text{T} = 150°\text{C}) \quad (16)$$

Columns with different dimensions, carrier gas type and flow rate can have substantially different t_M values. However, the optimal value of r in Eqs. (13) and (16), leading to the best trade-off between separation and time is approximately the same in all cases and is close to 0.4 [28]. Eq. (16) yields for optimal[1] R_T: $R_T = 12$ °C/t_M. The heating rate (R_T) in actual GC analyses might be optimal or not. However, expressing it in units of °C/t_M (rather than in °C/min) is always convenient when R_T values in different columns under different operational conditions are compared.

The choice of temperature program in this study was dictated not by optimization of the separation-time trade-off, but for simplicity of predicting the peak mapping in GC × GC separation space. It has been shown elsewhere [29] that, in a balanced temperature program where the heating ramp is preceded by a temperature hold lasting for a few void times (depending on the heating rate), all solutes eluting during the ramp elute with the same retention factor. Specifically, when $r = 0.6$ (i.e., according to Eqs. (13) and (16), when $R_T = 18$ °C/t_M), all solutes eluting during the ramp, elute with k close to $k = 1$. Therefore, the elution temperature (^1T_e) of each solute eluting from the primary column is equal to its characteristic temperature:

$$^1T_e = {}^1T_{char} \quad (17)$$

The retention factor in the secondary dimension can be found from Eq. (5) which, when each solute temperature (T) is close to its T_{char}, can be approximated as [24,25,28]:

$$lnk = -\frac{T - T_{char}}{\theta_{char}} \quad (18)$$

In typical GC × GC analysis, the temperature increase during each secondary run does not exceed 1 °C. As a result, each such run can be viewed as being isothermal. Therefore, assuming that both columns are always at the same temperature, the isothermal temperature (^2T) of the compounds analysed in each secondary run is equal $^1T_{char}$. We can therefore replace T in Equation (18) above with $^1T_{char}$, replace T_{char} with $^2T_{char}$ (the characteristic temperature of the analyte on the secondary column), and replace θ_{char} with $^2\theta_{char}$ (the characteristic thermal constant of the analyte on the secondary column). The resulting equation provides the retention factor of an analyte on the secondary column during a fast, effectively isothermal separation, ^2k:

[1] Optimal R_T is 12 C/t_M when t_M is measured at 150 °C. Typically, however, t_M is measured at initial temperature (T_i) of the heating ramp which is typically lower than 150 °C yielding lower t_M. To be 12 C/t_M at 150 °C, R_T at T_i should be close to 10 C/t_M as recommended in literature [28].

$$\ln^2 k = -\frac{{}^1T_{char} - {}^2T_{char}}{{}^2\theta_{char}} \quad (19)$$

Once ${}^2k$ is calculated, estimates of second-dimension retention times, ${}^2t_R$, can be obtained with the following equation:

$${}^2t_R = {}^2t_M\left({}^2k + 1\right) + {}^2t_M \quad (20)$$

where ${}^2t_M$ is the second-dimension void time (estimated at 150 °C) and ${}^tt_M$ is the void time of the fused silica transfer line connecting the second dimension column to the detector (see Section 2.2 for details on instrumentation used in this study).

Characteristic parameters can be used to model second-dimension retention factors as illustrated by Equation (19) and by extension, the distribution (the mapping) of compounds in a GC × GC separation space, as this paper demonstrates. The underlying assumption for using Eq. (19) in the mapping is that each solute elutes from the primary column at the temperature (${}^1T_e$) equal to the solute characteristic temperature (${}^1T_{char}$) in the primary column. This assumption is different to some degree from the reality and can be viewed as the first approximation. However, as illustrated below, the distribution maps based on Eq. (19) are reasonably close to their experimental counterparts. Accounting for the difference ${}^1T_e - {}^1T_{char}$ in future studies can lead to more accurate mapping. The difference in a balanced single-ramp temperature program can be estimated as [25]:

$$T_e - T_{char} = \theta_{char}\ln(e^r - 1) \quad (21)$$

The difference between T_e and T_{char} disappears, i.e. $T_e = T_{char}$ when

$$r = \ln 2 \quad (22)$$

2. Materials and methods

2.1. Standards

A Programmed Test Mix (Sigma-Aldrich, Oakville, ON, Canada), known more commonly as the Grob Test Mix, was diluted 1 in 4 in dichloromethane (Sigma-Aldrich) so that the concentrations of its components ranged from about 70 μg mL^{-1} to 133 μg mL^{-1}. This mixture was separated under the GC × GC conditions described below. The following compounds from this mixture were used for this study: decane, 1-octanol, undecane, 2,6-dimethylaniline, methyl decanoate and methyl dodecanoate.

A diesel range organics mixture (DRO) (Restek Corporation, Bellefonte, PA, USA) was diluted to give concentrations of about 100 μg mL^{-1} in dichloromethane (Sigma-Aldrich) and separated under the conditions described below. From this mixture, the following components were chosen for this study: dodecane, tetradecane, hexadecane, octadecane and eicosane.

Twenty-eight other compounds from existing in-house solutions were chosen and diluted to about 100 μg mL^{-1} in dichloromethane. These included, 1,4-dimethylnaphthalene, 1-tetradecanol, 2,3-dimethylaniline, 2,5-dichlorophenol, 2,6-dichlorophenol, 2-decanone, 2-heptanone, 2-nonanol, 2-nonanone, 2-octanone. 2-tridecanone, 3-octanone, 3-*tert*-butylphenol, 4-*sec*-butylphenol, 4-*tert*-butylphenol, 5-nonanol, anthracene, bipheyl, decanal, naphthalene, *N*-ethylaniline, octanal, *p*-ethylaniline, phenanthrene, tributylphosphate, trimethylphosphate, tripropylphosphate and undecanal. Compounds were chosen to represent a wide range of analyte chemistries, intermolecular interactions and elution temperatures.

2.2. Instrumentation

All separations were carried out using an Agilent 7890A gas chromatograph (Agilent Technologies, Mississauga, ON) equipped with a split/splitless injector, flame ionization detector and a consumable-free dual stage/quad-jet thermal modulator (Leco Corporation. St. Joseph, MI, USA). Injections of 1 μL were performed in split mode using a split ratio of 25:1, an inlet temperature of 275 °C and He carrier gas (5.0 grade, Praxair, Edmonton, AB). The inlet was operated in constant flow mode at 2.0 mL min^{-1} to assess if the model generates good maps under pneumatic conditions similar to normal GC × GC runs. Five different stationary phase combinations were studied (all columns were from Restek, PA) and are shown in Table 1 along with the heating rates that corresponded to 18 °C t_M^{-1} for that combination. Every chromatographic column used had an inner diameter of 0.25 mm. For each combination, a fused silica transfer line (Agilent, ON) of 0.18 m × 0.2 mm connected the secondary column to the detector (FID collecting at 200 Hz).

Rtx-5MS is a low polarity 5% diphenyl, 95% dimethyl polysiloxane phase, Rtx-200(MS) is a mid-polarity, trifluoropropylmethyl polysiloxane phase, and Rxi-17Sil MS is a mid-polarity phase with 50% diphenyl 50% dimethypolysiloxane-like characteristics. Rough preliminary studies using just 16 compounds and Stabilwax (Restek, PA), a polyethylene glycol column, as the second dimension were carried out prior to the work presented here. The results of said preliminary study are presented in the supplemental information and helped to guide the design of experiments shown in this paper.

In all temperature programs, the heating ramp was preceded by an initial $3t_M$-long hold making the programs to be close to the balanced ones [29]. All compounds eluting during the initial hold were considered as having too little retention on the primary stationary phase for the model to be applied. Additionally, in all experiments and in theoretical predictions, modulator and secondary oven were, after the initial hold, at about the same temperatures. For each combination, the initial temperature for the primary oven was 40 °C. The final temperature was 320 °C in analyses with Rtx-200(MS) secondary columns, and 330 °C – with Rtx-5MS and Rxi-17Sil MS secondary columns. In all cases, the final hold lasted for 10 min. The initial temperatures of the modulator and the secondary oven differed from the primary oven and from each other because the ChromaTOF software (Leco Corporation) demands an

Table 1
GC × GC stationary phase configurations upon which separations were performed.

Combination	1° column	2° column	1° Length (m)	2° Length (m)	1° d_f (μm)	2° d_f (μm)	t_M (min)	Heating rate (°C min^{-1})	Effect
A	Rtx-5MS	Rtx-200MS	30.55	0.34	0.25	0.25	1.12_1	16.05	"Default"
B	Rtx-5MS	Rtx-200	30.55	0.34	0.25	0.50	1.12_1	16.05	Lower 2° β
C	Rtx-5MS	Rtx-200MS	30.55	0.35	0.50	0.25	0.93_3	19.30	Lower 1° β
D	Rtx-200MS	Rtx-5MS	24.70	0.35	0.25	0.25	0.77_4	23.26	Reverse polarity
E	Rtx-5MS	Rxi-17Sil MS	30.55	0.35	0.25	0.25	1.12_1	16.05	Change 2° selectivity

offset of at least 3 °C between the primary and secondary ovens, and at least 8 °C between the primary oven and the modulator. Therefore, the secondary oven was set to an initial temperature of 45 °C and the modulator was set to an initial temperature of 48 °C. Both were held so that all three of these heated zones would be at about the same temperature from 48 °C until the end of the run. Modulation periods, P_M, of 1.5 s were used for combinations A, C, and E with a hot pulse time of 0.3 s. For combinations B and D, a P_M of 2.0 s was used with a hot pulse time of 0.4 s (this larger P_M was used to avoid wraparound on secondary stationary phases expected to have stronger retention).

3. Results and discussion

In order to assess the feasibility of using characteristic parameters to map compound distribution in GC × GC space, experiments were performed to cause molecules to elute from the primary column at approximately their characteristic temperatures. Assuming a typical ${}^1\theta_{char}$ of ~30 °C, all experiments were conducted using temperature programming rates of 18 °C t_M^{-1}. It is important to note that because a non-selective detector was used (an FID), analyses of all 39 compounds were not carried out at the same time but in small batches (and sometimes individually) in order to ensure confidence in the identification of each compound. Hence, experimental chromatograms shown in here are plotted as peak apex plots using retention time data from the peak tables of each run.

3.1. Generating distribution maps from characteristic parameters

Maps showing expected analyte distributions on the combinations shown in Table 1, were generated with an in-house MATLAB (The MathWorks Inc., Natick, MA, USA) script. The script calculated characteristic parameters using Equations (9) and (10) with thermodynamics-based parameters (*A, B* and *C*) obtained using the approach of Hou et al. [11]. All parameters are available in the supplemental information, Tables S1, S2a and S2b. Additionally, figures showing maps and experimental data with each compound identified by an assigned number are available for all investigated combinations, in the supplemental information. Identifying numbers were omitted from figures presented in the main body of the manuscript to ensure clarity of retention patterns due to figure sizing.

Figs. 1–3a illustrate the creation of useful maps for guiding chromatographers' column choice for GC × GC separations, using Combination A from Table 1.

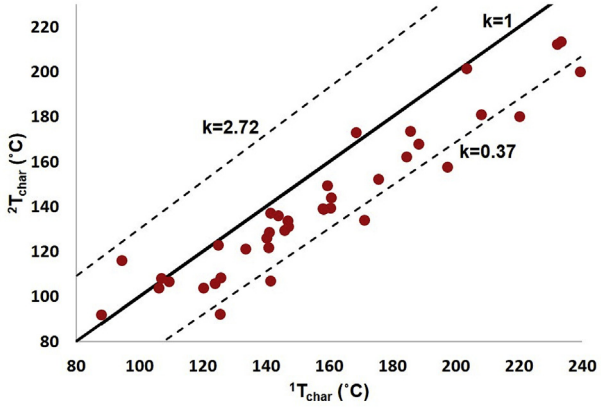

Fig. 1. Calculated characteristic temperatures of thirty-nine compounds on Combination A; Rtx-5MS × Rtx-200MS ($^1\beta$ and $^2\beta = 250$).

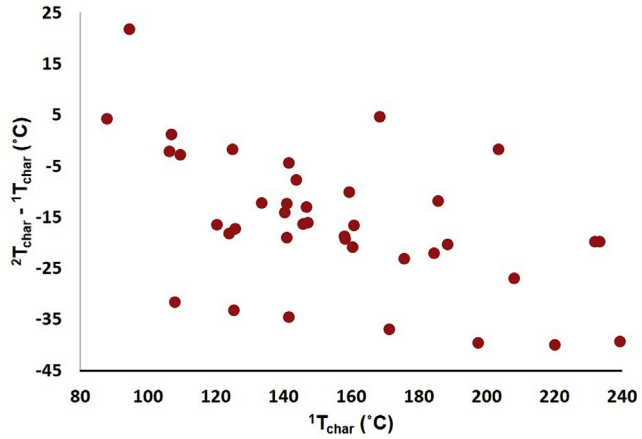

Fig. 2. Rotation of Fig. 1 by 45° in a clockwise direction, presenting the distribution in a format more similar to a GC × GC chromatogram.

Fig. 1 shows a plot of ${}^2T_{char}$ vs. ${}^1T_{char}$ for Combination A in which both columns have phase ratios, β, of 250. This plot, although admittedly unintuitive to read, contains a great deal of useful information. The black solid diagonal line in this figure is the ${}^2k = 1$

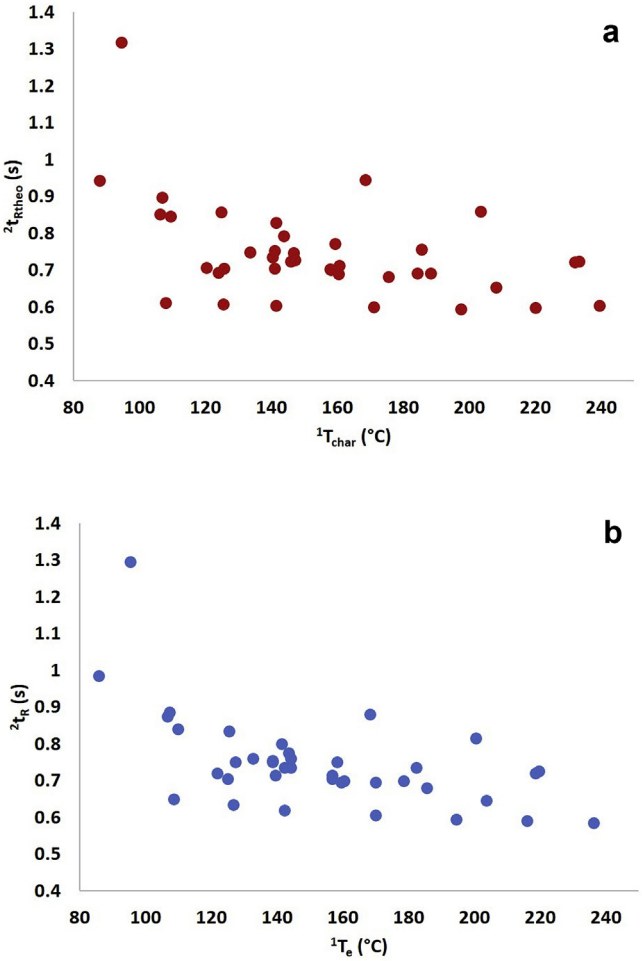

Fig. 3. a: Calculated map of the thirty-nine compounds on the Combination A GC × GC separation space ($^1\beta$ and $^2\beta = 250$). b: Experimental map of the thirty-nine compounds and their primary elution temperatures as determined on the Combination A GC × GC separation space ($^1\beta$ and $^2\beta = 250$).

line; any compounds falling along this line can be expected to elute from both columns at their characteristic temperatures. The upper, dashed diagonal line is the ${}^2k = 2.72$ line and lies at a vertical distance of ~${}^2\theta_{char}$ above the ${}^2k = 1$ line. Compounds eluting along this line are expected to elute from the second-dimension column with ${}^2k \approx 2.72 \approx {}^2k_{char} \times e$ (Euler's number) and would therefore show strong affinity for the secondary column. A secondary oven offset of about $+{}^2\theta_{char}$ should cause these compounds to elute with ${}^2k \approx {}^2k_{char} \approx 1$. Conversely, the lower dashed diagonal line is the ${}^2k = 0.37$ line, lying at ~${}^2\theta_{char}$ below the ${}^2k = 1$ line. Molecules sitting on this line should elute with ${}^2k \approx {}^2k_{char}/e$, and a secondary oven offset of about -${}^2\theta_{char}$ should cause these compounds to be more strongly retained on the secondary column, eluting with ${}^2k = {}^2k_{char}$. Plots like Fig. 1 provide useful insight for guiding temperature offsets and manipulating ${}^2k$ for given molecules of interest. More dashed "${}^2k$ lines" can be added to the figure as needed, note also that said lines are not parallel as θ_{char} generally increases with T_{char}.

Fig. 1 is transformed into a more easily interpreted form by rotating the Fig. 45° clockwise (i.e. make the $k = 1$ line horizontal by plotting ${}^2T_{char} - {}^1T_{char}$ vs. ${}^1T_{char}$). The result is Fig. 2, which has an appearance similar to a GC × GC chromatogram.

However, the aim is to generate maps that provide a visual of analyte distribution across the separation space. Figs. 1 and 2 do not account for how each compound's individual ${}^2k$ changes with temperature. However, Equation (19) permits the inclusion of this factor through the estimation of ${}^2k$ using both primary and secondary T_{char} as well as ${}^2\theta_{char}$. Furthermore, greater visual similarity between the maps and actual chromatograms can be obtained by using the estimated ${}^2k$ with estimates of second-dimension void time, ${}^2t_M$, and transfer line travel time, ${}^tt_M$, to roughly calculate second-dimension retention time, ${}^2t_R$, using Equation (20). For this work, void times were estimated using LECO GC × GC calculator (Leco, MI) but these can be estimated using any commercial or in-house flow calculator. Note also that for the maps shown in this paper, void times were calculated at 150 °C. Fig. 3a shows the resulting map when Fig. 2 is transformed by Equations (19) and (20), while Fig. 3b shows the corresponding experimental retention data (Combination A from Table 1).

Fig. 3a and b shows that distribution and relative retention times of compounds in the experimental map closely match that of the theoretical map indicating that the mapping based solely on characteristic parameters in Eq. (19) can be sufficient for outlining the separation space of GC × GC analysis. The mapping can be further improved if departures of solute elution temperatures from their characteristic temperatures in temperature-programmed primary column are taken into account.

Table 2 contains the differences between the characteristic temperature of each compound on the primary column, ${}^1T_{char}$, and their elution temperatures, ${}^1T_e$, on that column for Combination A. It also contains the differences between their theoretical secondary retention times, ${}^2t_{Rtheo}$, calculated from Equation (19) and their experimental secondary retention times, ${}^2t_R$.

What are the theoretical expectations for the differences

Table 2
Differences between ${}^1T_{char}$ and ${}^1T_e$, and between ${}^2t_{Rtheo}$ and ${}^2t_R$ for combination A

Assigned number	Compound	${}^1T_{char} - {}^1T_e$ (°C)	${}^2t_{Rtheo} - {}^2t_R$ (s)
1	1,4-dimethylnaphthalene	5.9	−0.01
2	1-octanol	−1.5	−0.01
3	1-tetradecanol	4.4	0.01
4	2,3-dimethylaniline	2.5	−0.01
5	2,5-dichlorophenol	1.4	−0.01
6	2,6-dichlorophenol	2.9	−0.01
7	2,6-dimethylaniline	2.4	0.00
8	2-decanone	0.0	0.03
9	2-heptanone	2.1	−0.04
10	2-nonanol	−1.7	−0.05
11	2-nonanone	−0.6	0.02
12	2-octanone	−0.4	0.01
13	2-tridecanone	3.1	0.02
14	3-octanone	−0.4	−0.02
15	3-*tert*-butylphenol	1.2	0.00
16	4-*sec*-butylphenol	0.8	−0.01
17	4-tertbutylphenol	1.4	−0.02
18	5-nonanol	−1.1	−0.01
19	anthracene	13.5	0.00
20	bipheyl	5.6	−0.01
21	decanal	0.3	0.02
22	decane	−0.7	−0.04
23	dodecane	−0.8	−0.02
24	eicosane	3.2	0.02
25	hexadecane	2.9	0.00
26	methyl decanoate	0.3	0.01
27	methyl dodecanoate	2.7	0.01
28	naphthalene	3.5	−0.01
29	*N*-ethylaniline	0.8	−0.01
30	octadecane	4.1	0.01
31	octanal	−0.4	0.01
32	*p*-ethylaniline	1.6	−0.02
33	phenanthrene	13.4	0.00
34	tetradecane	1.1	−0.01
35	tributylphosphate	2.9	0.05
36	trimethylphosphate	−0.9	0.02
37	tripropylphosphate	0.1	0.06
38	undecanal	1.1	0.02
39	undecane	−1.3	−0.03

between ${}^1T_e$ and ${}^1T_{char}$? Consider, e.g., the solutes with ${}^1T_{char} = 150\,^\circ C$. As noted earlier, the nominal θ_{char} for these solutes is, Eq. (14), ${}^1\theta_{char,nom} = 30\,^\circ C$. The actual θ_{char} values of these solutes are bound by inequalities $21\,^\circ C \leq \theta_{char} \leq 39\,^\circ C$. One can find from Eq. (13) that, at the heating rate of $R = 18\,^\circ C/t_M$ in our experiments, $0.46 \leq r \leq 0.86$. Eq. (21) yields:

$$-6.4\,^\circ C \leq {}^1T_{char} - {}^1T_e \leq 20.8\,^\circ C \quad (23)$$

According to Eq. (14), solutes with larger ${}^1T_{char}$ have larger ${}^1\theta_{char,nom}$ and, therefore, awider window, Eq. (15), of possible ${}^1\theta_{char}$ values eventually causing a wider window of possible differences ${}^1T_{char} - {}^1T_e$. One can conclude that these differences in Table 2 are well within theoretical expectations. One can also notice that the window for the differences ${}^1T_{char} - {}^1T_e$ in Eq. (23) is not symmetric relative to zero, but shifts upwards. Consequently the window for these differences in Table 2 increases as well. Confined within the range (−1.7 °C, 13.5 °C) in Table 2, the differences correspond (at the heating rate of 16.05 °C/min, Table 1) to retention time differences within the range (−6.4 s, 50.5 s).

The differences between ${}^1T_{char}$ and ${}^1T_e$ also affect the differences, ${}^2t_{Rtheo} - {}^2t_R$, between theoretical and experimental retention times in the second dimension. When assessing these values (${}^2t_{Rtheo} - {}^2t_R$), for all combinations shown in this study, it is important to consider two factors.

1) The values of ${}^2t_M$ and ${}^t t_M$ used in the calculations of ${}^2t_{Rtheo}$ are estimates of the void times of the second-dimension column and the transfer line at 150 °C (the same temperature used to determine the heating rate that would theoretically cause compounds to elute with ${}^1T_e = {}^1T_{char}$). However, over the course of a constant-flow programmed-temperature separation on this column set, ${}^2t_M$ would range from about 0.45 s at 90 °C to 0.29 s at 320 °C while ${}^t t_M$ would range from about 0.14 s at 90 °C to 0.09 s at 320 °C.
2) The maps are not (yet) built to accurately predict retention times but to serve as a rapid, easy-to-generate visual aid for guiding column choice selection prior to optimizing instrumental conditions in GC × GC experiments. Further refinement would be required to use these characteristic parameters and any values derived from them as accurate predictors of retention times (and by extension to use their predictions for optimizing instrument conditions). It should be possible to acquire more meaningful estimates of ${}^2t_R$ for prediction purposes by accurately calculating the outlet pressures at both the primary and secondary column throughout the separation in order to estimate the values of ${}^2t_M$ and ${}^t t_M$ at the time when each compound elutes from the primary and secondary columns respectively. The estimates of these values (${}^2t_M$ and ${}^t t_M$) used in this paper, however, are extremely useful for quickly (with little computational time and complexity) generating maps that answer the question "would these two columns, with these stationary phases and phase ratios, arranged in this order be a good choice for GC × GC separation of this sample?". The values of ${}^2t_{Rtheo}$ calculated here do not carry much meaning beyond their utility for generating maps that serve the purpose outlined above. Indeed, maps could be made using only the calculated values of ${}^2k$, and still serve their intended purpose. However, going one step further and roughly estimating ${}^2t_{Rtheo}$ allows for easier comparison of the generated maps and the experimental data. At this stage, the significance of the magnitude of any numerical differences between these values and the actual ${}^2t_R$ values was ignored.

3.2. Effects of changing phase ratio, polarity order and selectivity

3.2.1. Combination B – reduced 2° phase ratio

Fig. 4a shows theoretical maps of Combinations A and B. The experimental data for these Combinations is plotted in Fig. 4b. The expected upward shift in ${}^2t_{Rtheo}$ going from Combination A to Combination B (i.e. decreasing the phase ratio and increasing retention on the secondary column) is demonstrated on theoretical map and supported by the experimental data. The upward shift on the theoretical map is slightly greater than that observed experimentally. These differences are largest at higher temperatures so the overestimation of ${}^1t_M$ likely plays a role.

Tables showing values for ${}^1T_{char} - {}^1T_e$ and ${}^2t_{Rtheo} - {}^2t_R$, for this and all other combinations studied are available in the supplemental information. In summary, values of ${}^1T_{char} - {}^1T_e$ for Combination B are similar in magnitude to those for Combination A while ${}^2t_{Rtheo} - {}^2t_R$ for all compounds is positive and notably larger on average for Combination B.

3.2.2. Combination C – reduced 1° phase ratio

A reduction in primary phase ratio, ${}^1\beta$, from 250 to 125 while maintaining a secondary phase ratio, ${}^2\beta$, of 250, is expected to cause compounds to show increased retention on the primary column; ${}^1t_R$ will shift to the right. This, in turn, would cause compounds to meet the second dimension column at a higher temperature and

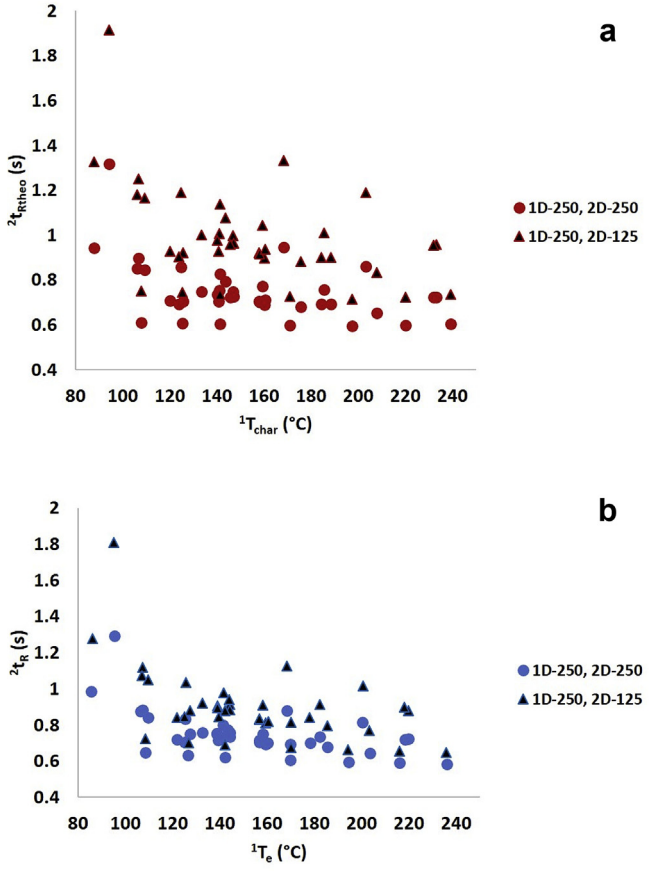

Fig. 4. a Map showing the theoretical shift in retention of thirty-nine on Combination B; ${}^2\beta$ is reduced from 250 to 125 while ${}^1\beta$ remains unchanged. b Experimental map of thirty-nine compounds on Combination B; ${}^2\beta$ is reduced from 250 to 125 while ${}^1\beta$ remains unchanged.

elute with lower ^{2}k. The map generated for Combination C demonstrates this expected behaviour as shown in Fig. 5a and is supported by experimental data shown in Fig. 5b.

Briefly, the values of $^{1}T_{char} - {}^{1}T_{e}$, are much larger for this combination than for Combinations A and B likely on account of the θ_{char} values on this thicker film (smaller phase ratio) Rtx-5MS phase being greater than nominal θ_{char} for the corresponding phase chemistry with a phase ratio of 250. $^{2}t_{Rtheo} - {}^{2}t_{R}$ are small and a mixture of negative and positive values.

3.2.3. Combination D – polar/apolar configuration

Fig. 6a and b shows the map and experimental data, respectively for Combination D. This combination, which places the more polar column in the first dimension and the apolar column in the second dimension, was the most poorly mapped with $^{1}T_{char}$ being smaller than $^{1}T_{e}$ for most compounds (i.e. compounds eluted from the primary column at higher temperature than expected). On this phase, most compounds had $^{1}\theta_{char}$ values at about or well below their nominal values. It is also worth noting that the compounds that eluted at a lower temperature than expected have $^{1}\theta_{char}$ values above their nominal values. The alkanes are particularly poorly mapped and this might be associated with low retention near the start of the run on this more polar phase. Overall, however, the compounds on Combination D were mapped in a manner that agrees well with the experimental results – the relative positions of compounds still sufficiently match the experimental data to inform decisions about the utility of this combination.

3.2.4. Combination E – change 2° phase chemistry

The last combination, Combination E, employs a column with 50% diphenyl and 50% PDMS like properties in the second dimension (Rxi-17Sil MS) instead of trifluoropropyl methylpolysiloxane (Rtx-200(MS)). It is mapped in Fig. 7a with experimental data shown in Fig. 7b. This combination is also well mapped. Magnitudes of differences between $^{1}T_{char}$ and $^{1}T_{e}$ are similar to those observed for Combinations A and B (that shared the same first-dimension column). Larger differences, like before, are associated with $^{1}\theta_{char}$ outliers. As with other combinations, this map does a good job of illustrating compound distribution for the chosen column chemistries and phase ratios and can aide chromatographers in making appropriate column choices.

Across all of these combinations, the maps serve as good indicators of the peak distribution and dimensions of the required separation space – thus providing helpful insight that a chromatographer can use in selecting stationary phases for their separation. They are fast to generate, as long as the thermodynamic parameters *A*, *B* and *C* for the compounds to be mapped are available. With further refinement, they could prove very useful for predicting retention times for the sake of optimizing experimental conditions.

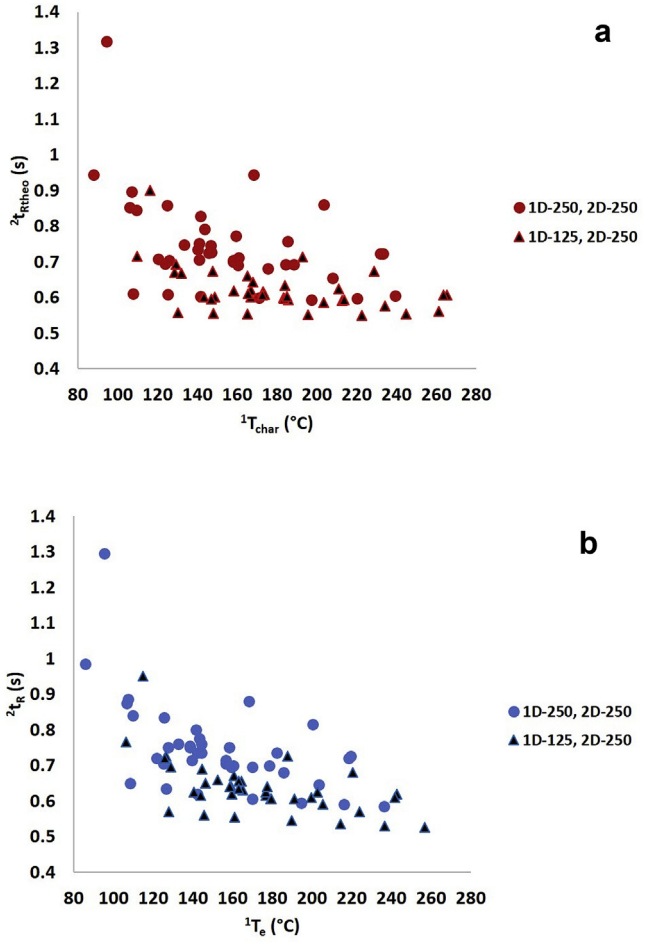

Fig. 5. a Map showing the theoretical shift in retention of thirty-nine on Combination C; $^{1}\beta$ is reduced from 250 to 125 while $^{2}\beta$ remains unchanged. b Experimental retention of thirty-nine compounds on Combination C; $^{1}\beta$ is reduced from 250 to 125 while $^{2}\beta$ remains unchanged.

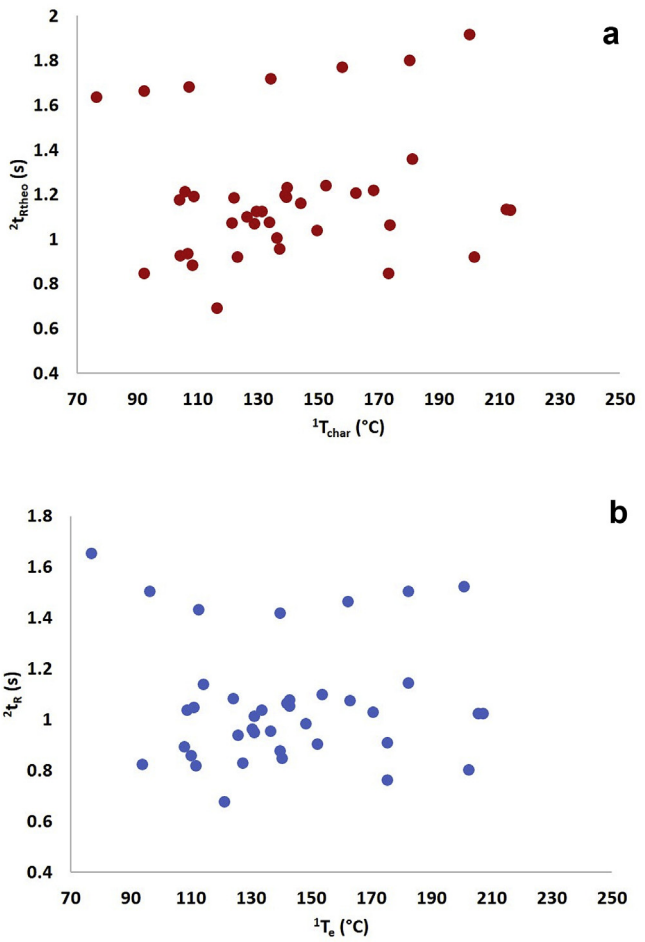

Fig. 6. a Map of the thirty-nine compounds on Combination D; polar/apolar configuration, $^{1}\beta$ and $^{2}\beta = 250$. b Experimental secondary retention times of the thirty-nine compounds and their primary elution temperatures as determined on Combination D; polar/apolar configuration, $^{1}\beta$ and $^{2}\beta = 250$.

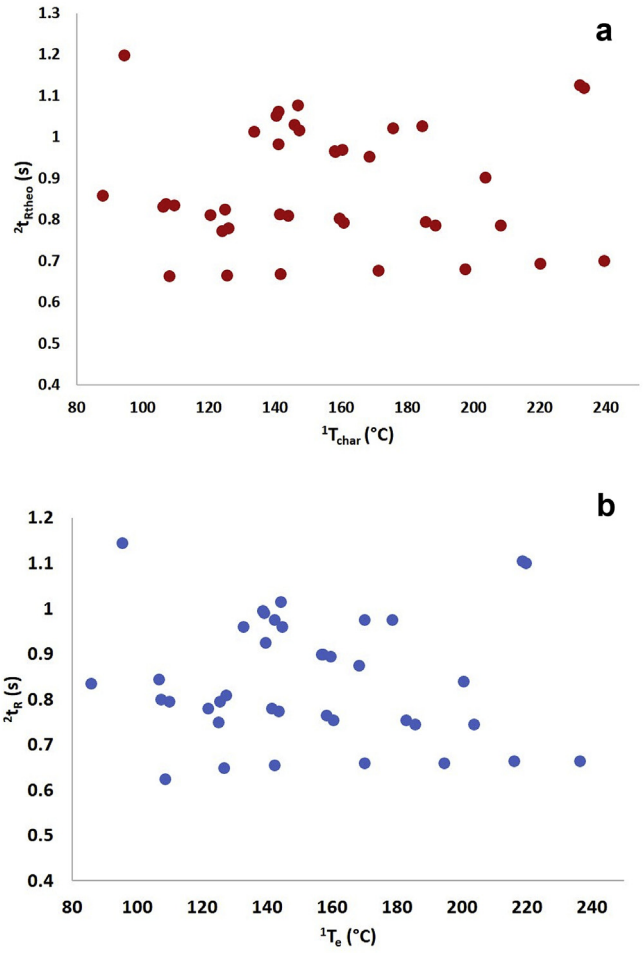

Fig. 7. a Map of the thirty-nine compounds on Combination E; 2° phase chemistry changed, $^1\beta$ and $^2\beta = 250$. b Experimental secondary retention times of the thirty-nine compounds and their primary elution temperatures as determined on Combination E; 2° phase chemistry changed, $^1\beta$ and $^2\beta = 250$.

Finally, this approach is easily extended to mapping comprehensive three-dimensional GC separations (GC × GC × GC). This is a concept which was first demonstrated in 2000 [30] and has since been revisited periodically in the literature [31–33]. By considering the ^{2}D and ^{3}D separations to be isothermal, ^2T_e is approximated as $^1T_{char}$ which is then used as T in Equation (18), while $^3T_{char}$ is used in place of T_{char} in a similar manner to the generation of the GC × GC maps previously. Following the approach for GC × GC maps, $\ln(^3k)$ can be estimated from Equation (19) and then plots of ^3k vs. ^2k vs. $^1T_{char}$ can be generated as maps of a GC × GC × GC space. We believe the approximation of isothermal separations in ^{2}D and ^{3}D is justified given that for the fastest ramp used in the present research, 23.26 Cmin^{-1}, even with a 2 s separation in ^{2}D, ^2T_e will only be about 0.8 C above $^1T_{char}$. A theoretical map for a GC × GC × GC separation, of the same 39 compounds used in this study, on a Rtx-5MS × Rtx-200MS × Rxi-17Sil MS, ($^1\beta = {}^2\beta = {}^3\beta = 250$) separation space are presented in the supporting information (Figs. S7a and S7b).

4. Conclusions

Characteristic thermodynamic parameters acquired through distribution-centric thermodynamic models provide useful and chromatographically meaningful parameters. They can be used to generate maps that guide stationary phase chemistry, stationary phase configuration and stationary phase ratio selection in GC × GC and potentially GC × GC × GC. With additional refinement, particularly with regards to the calculation of void times it should be possible to quickly and accurately predict and simulate GC × GC separations under more normal operating conditions, thereby allowing the optimization of combination of stationary phases and secondary temperature offsets.

Declaration of competing interest

The authors declare that they have no known competing financial interests or personal relationships that could have appeared to influence the work reported in this paper.

Acknowledgements

The authors wish to acknowledge the Natural Sciences and Engineering Research Council of Canada (NSERC) and the Partnership for Clean Competition for the financial support of this research.

Appendix A. Supplementary data

Supplementary data to this article can be found online at https://doi.org/10.1016/j.aca.2019.08.011.

References

[1] J. Harynuk, T. Górecki, Am. Lab. 39 (2007) 36–39.
[2] H. Snijders, H. Janssen, C. Cramers, J. Chromatogr. A 718 (1995) 339–355.
[3] H. Snijders, H. Janssen, C. Cramers, J. Chromatogr. A 756 (1996) 175–183.
[4] F. Aldaeus, Y. Thewalim, A. Colmsjö, J. Chromatogr. A 1216 (2009) 134–139.
[5] B. Karolat, J. Harynuk, J. Chromatogr. A 1217 (2010) 4862–4867.
[6] T.M. McGinitie, H. Ebrahimi-Najafabadi, J.J. Harynuk, J. Chromatogr. A 1330 (2014) 69–73.
[7] T.M. McGinitie, H. Ebrahimi-Najafabadi, J.J. Harynuk, J. Chromatogr. A 1325 (2014) 204–212.
[8] C.A. Claumann, A. Wüst Zibetti, A. Bolzan, R.A.F. Machado, L.T. Pinto, J. Chromatogr. A 1406 (2015) 258–265.
[9] C.A. Claumann, A. Wüst Zibetti, A. Bolzan, R.A.F. Machado, L.T. Pinto, J. Chromatogr. A 1425 (2015) 249–257.
[10] S. Hou, K.A.J.M. Stevenson, J.J. Harynuk, J. Sep. Sci. 41 (2018) 2553–2558.
[11] S. Hou, K.A.J.M. Stevenson, J.J. Harynuk, J. Sep. Sci. 41 (2018) 2559–2564.
[12] K.A.J.M. Stevenson, J.J. Harynuk, J. Sep. Sci. (42) (2019) 2013–2022. https://doi.org/10.1002/jssc.201801294.
[13] F.L. Dorman, P.D. Schettler, L.A. Vogt, J.W. Cochran, J. Chromatogr. A 1186 (2008) 196–201.
[14] T.M. McGinitie, J.J. Harynuk, J. Chromatogr. A 1255 (2012) 184–189.
[15] A.C.A. Silva, H. Ebrahimi-Najafadabi, T.M. McGinitie, A. Casilli, H.M.G. Pereira, F.R. Aquino Neto, J.J. Harynuk, Anal. Bioanal. Chem. 407 (2015) 4091–4099.
[16] S. Zhu, S. He, D.R. Worton, A.H. Goldstein, J. Chromatogr. A 1233 (2012) 147–151.
[17] S. Zhu, W. Zhang, W. Dai, T. Tong, P. Guo, S. He, Z. Chang, X. Gao, Anal. Methods 6 (2014) 2608–2620.
[18] A. Burel, M. Vaccaro, Y. Cartigny, S. Tisse, G. Coquerel, P. Cardinael, J. Chromatogr. A 1485 (2017) 101–119.
[19] E.C.W. Clarke, D.N. Glew, Trans. Faraday Soc. 62 (1966) 539–547.
[20] M. Roth, J. Novak, Macromolecules 19 (1986) 364–369.
[21] F.R. Gonzalez, A.M. Nardillo, J. Chromatogr. A 842 (1999) 29–49.
[22] F. Aldaeus, Y. Thewalim, A. Colmsjö, Anal. Bioanal. Chem. 389 (2007) 941–950.
[23] L.M. Blumberg, J. Chromatogr. A 1491 (2017) 159–170.
[24] L.M. Blumberg, M.S. Klee, Anal. Chem. 72 (2000) 4080–4089.
[25] L.M. Blumberg, Temperature-Programmed Gas Chromatography, Wiley-VCH, DE, 2011.
[26] N. Brenner, J.E. Callen, M.D. Weis (Eds.), Gas Chromatography, Academic Press, New York, 1962.
[27] L.M. Blumberg, M.S. Klee, Anal. Chem. 70 (1998) 3828–3839.
[28] L.M. Blumberg, in: C.F. Poole (Ed.), Gas Chromatography, Elsevier, Amsterdam, 2012, pp. 19–78.
[29] L.M. Blumberg, M.S. Klee, J. Chromatogr. A 918 (2001) 113–120.
[30] E.B. Ledford Jr., C.A. Billesbach, Q. Zhu, J. High Resolut. Chromatogr. 23 (2000) 205–207.
[31] N.E. Watson, H.D. Bahaghighat, K. Cui, R.E. Synovec, Anal. Chem. 89 (2017) 1793–1800.
[32] F.C. Wang, J. Chromatogr. A 1489 (2017) 126–133.
[33] D.V. Gough, H.D. Bahaghighat, R.E. Synovec, Talanta 195 (2019) 822–829.